

Magnetocohesion of nanowires

E. N. Bogacheck, A. G. Scherbakov, and Uzi Landman

School of Physics, Georgia Institute of Technology, Atlanta, Georgia 30332

(Received 1 May 2000)

The cohesive force and electronic conductance in nanowires modeled by soft- and hard-wall confining potentials, under the influence of a magnetic field (magnetocohesion) and in the linear and nonlinear (finite applied voltage) regimes, are studied. The appearance of force oscillations as a function of the magnetic field and their correlation with the corresponding characteristics of the electronic conductance are demonstrated. For materials with a strong Fermi-surface anisotropy (e.g., bismuth), it is predicted that when the crystallographic axis associated with the largest diagonal element of the effective-mass tensor is aligned along the direction of the wire, the cohesive force increases dramatically (by an order of magnitude) compared to the case when that axis is perpendicular to the wire direction.

I. INTRODUCTION

Formation of interfacial wires of atomic dimensions (nanowires) via elongation of contacts had been predicted through early molecular dynamics (MD) simulations¹ and observed experimentally^{1–13} using tip-based microscopy, pin-disk, and mechanical break junction techniques. Furthermore, it had also been found that the elongation mechanism of the wire involves an oscillatory variation of the pulling force¹ and that such oscillations are correlated⁴ with stepwise variations of the conductance through the wire.^{3(b),14} The energetics and mechanical response in nanowires as well as the electrical transport through them have been analyzed using MD simulations and electronic structure calculations^{1,9,15–18} as well as through the use of a jellium model^{19–21} and free-electron treatments,^{22–25} including semiclassical analysis.^{20,26} In addition, the nature of the oscillatory behavior of the elongation force and the conductance, originating from structural rearrangements in the wire in conjunction with modifications of the electronic structure, have also been analyzed with the same techniques.

Because of the nature of the preparation methods currently used to generate such three-dimensional (3D) nanowires, it is often difficult to obtain reproducibly the same well-defined structures of the wires from one experiment to another, unlike the case of lithographically fabricated two-dimensional wires controlled via voltage gates. Consequently, it is particularly desirable in investigations of such wires to explore the dependence of the wire's properties (mechanical and/or electrical) on external fields, including magnetic fields,^{27–30} finite bias voltage,^{31,32} electromagnetic radiation,³³ and thermal gradients,^{34,35} which may be varied in a controllable manner.

To this end, we study in this paper the cohesive force of metallic nanowires under the influence of a magnetic field (magnetocohesion) in the linear and nonlinear applied voltage regimes. Using a free-electron model for a wire described either by a hard-wall or by a soft-wall confining potential, we demonstrate the effect of a magnetic field on the oscillatory cohesion force and its correlation with the magnetic-field-induced variations of the electric conductance through the wire. Furthermore, for the soft-wall potential

model we investigate effects of the anisotropy of the Fermi surface of metals on the cohesive force of the nanowire. We show that for a bismuth wire the force oscillations are highest when the crystallographic axis corresponding to the largest diagonal element of the electron-mass tensor is parallel to the axis of the wire.

The paper is organized as follows. The theoretical model for calculation of the cohesive force in nanowires is described in Sec. II, and the results are discussed in Sec. III (hard-wall potential) and Sec. IV (soft-wall potential, with an application to bismuth wires). We offer a summary in Sec. V.

II. NANOWIRE COHESION: FORMALISM

The mechanical properties of nanowires may be characterized by the cohesive force F , that is, the force required to elongate the wire whose volume remains constant.¹ Such a force can be measured with atomic force microscopy (AFM) during stretching (or compression) of a contact between a tip and a surface,^{1,4,10} and it is given by

$$F = - \left(\frac{\partial \Omega}{\partial L} \right)_V , \quad (1)$$

where L is the length of the wire of volume V , and the grand-canonical potential Ω is given by

$$\Omega = -k_B T \sum_i \ln \left[1 + \exp \left(\frac{\mu - E_i}{k_B T} \right) \right] , \quad (2)$$

where k_B is the Boltzmann constant, T is the temperature, μ is the chemical potential, and the E_i are the electronic energy levels with the index i denoting a set of quantum numbers including spin.

In a cylindrical wire the energy levels of the electrons may be expressed as a sum of transverse, ϵ_ν , and longitudinal, $p_z^2/2m_{||}$, parts:

$$E_{\nu p_z} = \epsilon_\nu + \frac{p_z^2}{2m_{||}} , \quad (3)$$

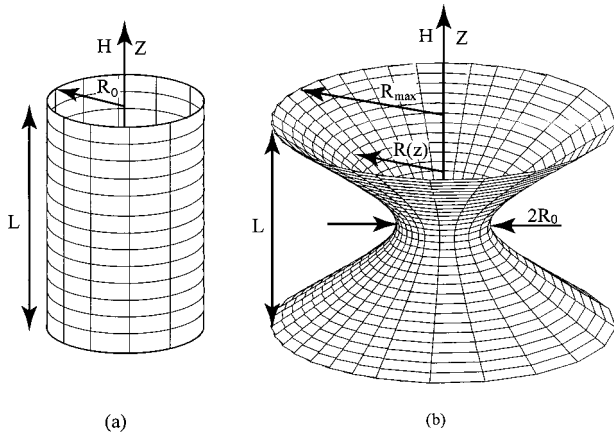


FIG. 1. Models of nanowires. (a) A nanowire of a uniform cylindrical shape. (b) A nanowire with a circular cross section but a variable axial shape described by the z dependence of the radius $R(z)=R_0+bz^2$ with $R_{\max}=\text{const}$; see Eq. (6).

where ν denotes a discrete set of quantum numbers, and m_{\parallel} is the electronic mass corresponding to the motion along the axis of the cylindrical wire. Introducing the density of states and integrating Eq. (2) twice by parts we get for a cylindrical wire

$$\Omega_{\text{cyl}}=-\frac{2L}{3\pi T}\left(\frac{2m_{\parallel}}{\hbar^2}\right)^{1/2}\times\sum_{\nu}\int dE(E-\epsilon_{\nu})^{3/2}\frac{e^{(E-\mu)/k_BT}}{(e^{(E-\mu)/k_BT}+1)^2}. \quad (4)$$

In a wire with a slowly (adiabatically)¹⁴ varying shape the cross-sectional radii depend on z (see below), and due to the z dependence of the transverse energy levels [ϵ_{ν} in Eq. (4)] we may define the thermodynamic potential of such a wire as

$$\Omega_{\text{wire}}=\frac{1}{L}\int_{-L/2}^{L/2}\Omega_{\text{cyl}}dz. \quad (5)$$

In the following we use this formalism for calculation of the cohesive force for nanowires modeled by different forms of the confining potential, and for field-free conditions as well as under the influence of a magnetic field.

III. HARD-WALL POTENTIAL MODEL

In the hard-wall potential model we consider nanowires with circular symmetry about the axis of the wires (z axis). A wire of length L may be modeled as a constriction of a uniform cylindrical shape, i.e., with a constant cross-sectional radius R_0 along the z axis [Fig. 1(a)], or as a constriction of variable shape [Fig. 1(b)]; in the latter case we assume that the cross-sectional radius $R(z)$ varies along the axis as (parabolic shape)

$$R(z)=R_0+(R_{\max}-R_0)\frac{(2z)^2}{L^2}, \quad -\frac{L}{2} \leq z \leq \frac{L}{2} \quad (6)$$

with the radius at the ends of the constricted section (that is, at the region connected to the leads), $R_{\max}\equiv R(\pm L/2)$, kept constant. We assume also that the volume of the constricted

region, V , remains constant during elongation of the wire in accordance with the results of molecular dynamics simulations.¹ In this model all the geometrical parameters depend only on the length L of the wire. In the case of an adiabatically slow variation of $R(z)$ we can divide the wire into thin cylindrical slices with radii $R(z)$ and then use Eq. (5) for the calculation of the thermodynamic potential.

In the absence of a magnetic field, and for a hard-wall confinement on the surface of the circularly symmetric wire, the transverse energy levels $\epsilon_{mn}^{(0)}$ in a cylindrical slice with the radius $R(z)$ described by Eq. (6) are given by (in this section we consider nanowires made from metals with a quadratic and isotropic dispersion law)

$$\epsilon_{mn}^{(0)}=\frac{\hbar^2\gamma_{mn}^2}{2m_{\perp}R^2(z)}. \quad (7)$$

Here, $m=0,\pm 1,\dots$ and $n=1,2,\dots$ are the azimuthal and radial quantum numbers, respectively, and m_{\perp} is the effective mass of the electrons corresponding to the motion in the plane perpendicular to the axis of the wire. The zeros of the Bessel function γ_{mn} determine the positions of single or double steps (depending on the m degeneracy of the energy levels) of the conductance¹⁴ and the oscillations of the cohesive force.^{19–25} In a longitudinal magnetic field (H) the electronic energy levels are computed²⁹ from the zeros of the confluent hypergeometric function

$$\mathcal{F}\left(-\left(\frac{k_{mn}^2R^2(z)}{4\alpha(z)}-\frac{|m|+m+1}{2}\right), |m|+1, \alpha(z)\right)=0, \quad (8)$$

where $k_{mn}^2=2m_{\perp}\epsilon_{mn}[R(z)]/\hbar^2$ and $\alpha=\pi R^2(z)H/\phi_0$ is the z -dependent magnetic flux in the wire expressed in units of the flux quantum $\phi_0=hc/e$.

From Eqs. (5)–(8) the magnetic field dependence of the cohesive force [Eq. (1)], arising from an elongation of the nanowire, can be calculated (in this section we neglect magnetic-field-induced spin effects). Such dependence on the wire's length L along with that of the conductance of the wire³⁶ is displayed in Figs. 2 and 3 for several values of the applied magnetic field (expressed in units of the dimensionless flux ϕ/ϕ_0); in these figures we show results for nanoconstrictions with $k_F R_{\max}=6$ and $k_F R_{\max}=4$, corresponding, respectively, to five and one conducting channels at zero field [see solid lines in Figs. 2(a) and 3(a)]. The main effect of the magnetic field on the force is to modify the oscillatory pattern [which exists already in zero field; see solid lines in Figs. 2(b) and 3(b)], including the appearance of new peaks. This effect, which is correlated with variations in the wire's conductance [compare panels (a) and (b) in Figs. 2 and 3], originates from magnetic-field-induced removal of degeneracies and shifts of the electronic transverse energy levels in the nanowire. Since the force can be influenced both by an applied magnetic field and/or by changes in the wire's length we show in Figs. 2(c) and 3(c) the force as a function of both ϕ/ϕ_0 and L . For wires made from normal metals the amplitude of the force oscillations is of the order of nanonewtons, nN. For nanowires made of such metals with only a few conducting channels (i.e., narrow wires), very high magnetic fields are required in order to achieve a magnetic flux of the order of ϕ_0 in the cross section of the nanowire. On the other

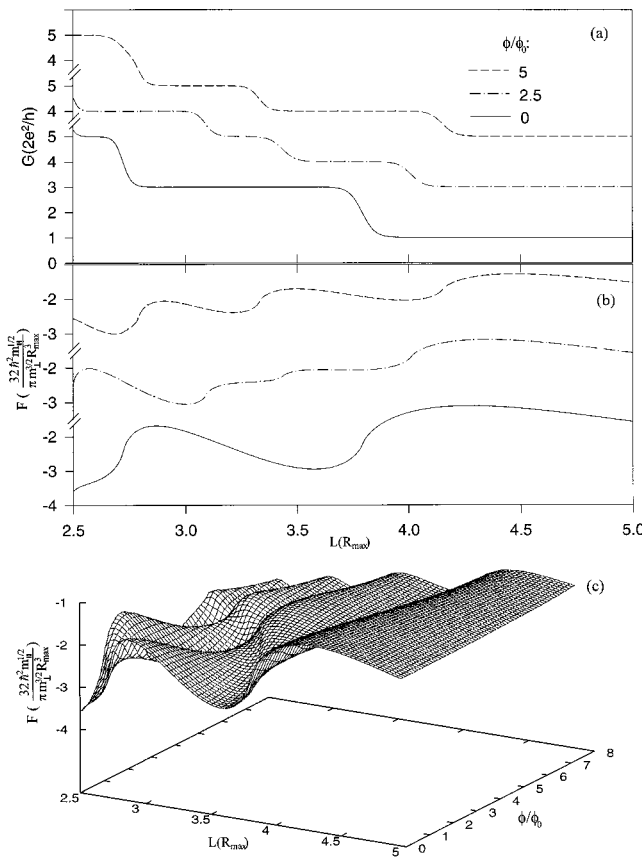


FIG. 2. (a) Conductance (G , in units of $2e^2/h$) and (b) cohesive force (F , in units of $32\hbar^2m_{||}^{1/2}/\pi m_{\perp}^{3/2}R_{\max}^3$) of a 3D wire, modeled via a hard-wall confining potential with a variable shape [Fig. 1(b)], plotted vs its dimensionless length L/R_{\max} with $k_F R_{\max}=6$. The different curves correspond to the marked values of the dimensionless magnetic flux $\phi/\phi_0=H\pi R^2/(hc/e)$. (c) The cohesion force plotted vs L/R_{\max} and ϕ/ϕ_0 .

hand, for semimetallic (bismuth-type) wires a magnetic flux of several ϕ_0 is readily achievable, while the amplitude of the force oscillations for such wires is smaller (see the next section).

The highest sensitivity of the cohesive force to the applied magnetic field occurs in the vicinity of changes in the wire's conductance (close to a step rise; see Figs. 2 and 3), that is, for conditions where the highest transverse energy (conductance channel) in the wire is located near the Fermi energy. Such conditions can be achieved through mechanical manipulation²⁹ of the wire or via application of a finite voltage;³² the latter, being an independent external parameter, may allow measurements of the mechanical and transport characteristics in a reproducible way. To demonstrate the combined effect of a finite bias voltage U and an applied magnetic field on the cohesion force we consider the cylindrical wire shown in Fig. 1(a). The thermodynamics of the wire may be described in terms of different effective electrochemical potentials for opposite-moving electrons.³² With the assumption that the wire is symmetric and that the potential drop takes place in the vicinity of the wire's ends (that is, near the contacts to the reservoirs), the thermodynamic potential may be written as

$$\Omega_{\text{cyl}}=\frac{1}{2}[\Omega(\mu_+-E_i)+\Omega(\mu_--E_i)], \quad (9)$$

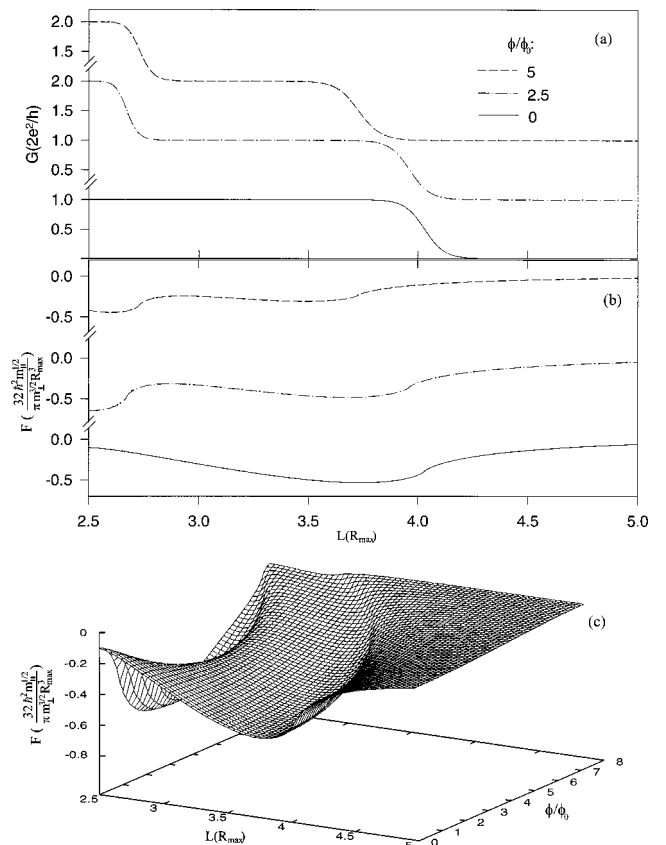


FIG. 3. Same as Fig. 2, but for a 3 D wire with $k_F R_{\max}=4$.

where $\mu_{\pm}=\mu\pm eU$. By taking the derivative of Ω_{cyl} with respect to wire length L , the magnetocohesion of the nanowire in the nonlinear (finite applied voltage) regime can be calculated.

In Fig. 4(a) we show the magnetic field dependence of the force at different values of an applied voltage (expressed in units of eU/ϵ_F) for a wire with $k_F R_0=5$, corresponding to three conducting channels at $H=0$ and $U\rightarrow 0$. Indeed, these results illustrate that the oscillatory dependence of the force on the magnetic field may be significantly influenced by an applied voltage; see also Fig. 4(b) where the simultaneous dependence of the force on the magnetic field and the applied voltage is displayed. We remark also that, as seen from Fig. 4, with the use of a finite applied voltage, magnetocohesion effects may be observed at lower magnetic field values than otherwise.

IV. SOFT-WALL CONFINING POTENTIAL (FOCUSING ON BISMUTH WIRES)

In the previous section we discussed the cohesive force and conductance in nanowires modeled by a hard-wall confining potential. In this section we turn to nanowires modeled by a soft-wall harmonic potential of the form³³

$$U_z(x,y)=\frac{\mu}{R^2(z)}(x^2+y^2), \quad (10)$$

where the effective radius of the wire, $R(z)$, is given by Eq. (6). This model allows an analytic solution of the Schrödinger equation in a magnetic field. In addition, it is particu-

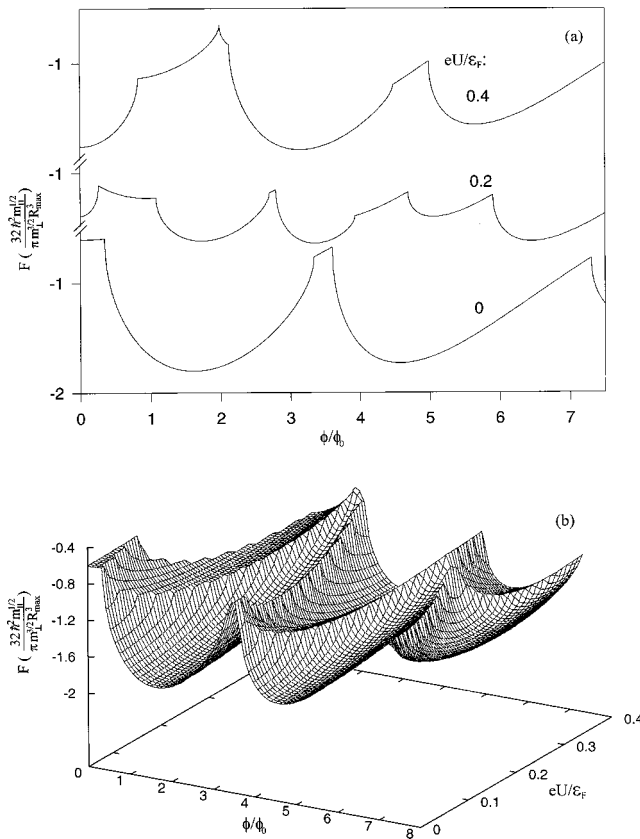


FIG. 4. (a) Cohesive force (F , in units of $32\hbar^2 m_{\parallel}^{1/2} / \pi m_{\perp}^{3/2} R_{\max}^3$) of a 3D wire, modeled via a hard-wall confining potential with a uniform cylindrical shape [Fig. 1(a)], plotted vs the dimensionless magnetic flux ϕ/ϕ_0 , with $k_F R_0 = 5$. Different curves correspond to the marked values of the applied voltage (U in units of ϵ_F/e). (b) The cohesion force plotted vs ϕ/ϕ_0 and eU/ϵ_F .

larly convenient for investigations of the effects of anisotropy of the electronic Fermi surface and may be applied to a study of bismuth nanowires. Consider the case of an ellipsoidal Fermi surface when one of the crystallographic axes (the z axis) is taken to be parallel to the axis of the wire. In a longitudinal magnetic field with the symmetric gauge for the vector potential, i.e.,

$$\mathbf{A} = \frac{1}{2}(-Hy, Hx, 0), \quad (11)$$

the Schrödinger equation corresponding to the transverse electronic motion in a cylindrical slice of radius $R(z)$ reads

$$\begin{aligned} & -\frac{\hbar^2}{2m_1} \left(\frac{\partial}{\partial x} - \frac{ieH}{\hbar c} y \right)^2 \psi - \frac{\hbar^2}{2m_2} \left(\frac{\partial}{\partial y} + \frac{ieH}{\hbar c} x \right)^2 \psi \\ & + \frac{\mu}{R^2(z)} (x^2 + y^2) \psi = \epsilon \psi, \end{aligned} \quad (12)$$

and the electronic energy is given by

$$E = \epsilon + \frac{p_z^2}{2m_3} \pm \frac{1}{2}g^* \beta H. \quad (13)$$

Here m_i ($i=1,2,3$) are diagonal elements of the effective-mass tensor, g^* is the effective g factor, $\beta = e\hbar/2m_0c$ is the Bohr magneton, and m_0 is the free-electron mass. The last term in Eq. (13) is the Zeeman interaction energy, which

takes into account spin effects in a magnetic field and may be of importance for bismuth wires because of possible large values of the effective g factor (see, for example, Ref. 37). Changing variables in Eq. (12) as $x = x_1(m_2/m_1)^{1/4}$ and $y = y_1(m_1/m_2)^{1/4}$, we obtain the Schrödinger equation for an electron with an effective (cyclotron) mass $m_{\perp} = (m_1 m_2)^{1/2}$ and an anisotropic potential

$$U_z(x, y) = \frac{1}{2}m_{\perp}(\omega_1^2 x_1^2 + \omega_2^2 y_1^2), \quad (14)$$

with the confining frequencies $\omega_{1,2}$ given by

$$\omega_{1,2}^2 = \frac{2\mu}{m_{1,2} R^2(z)}. \quad (15)$$

The transverse energy levels of the electron are expressed in terms of the frequencies $\omega_{1,2}$ (or diagonal mass elements $m_{1,2}$ corresponding to the axes perpendicular to the axis of the wire), and they are given by³⁸

$$\epsilon_{n_1 n_2} = \hbar \omega_+ (n_1 + \frac{1}{2}) + \hbar \omega_- (n_2 + \frac{1}{2}), \quad (16)$$

with

$$\omega_{\pm} = \frac{1}{2} \{ [\omega_c^2 + (\omega_1 + \omega_2)^2]^{1/2} \pm [\omega_c^2 + (\omega_1 - \omega_2)^2]^{1/2} \}. \quad (17)$$

Here, n_1 and n_2 are non-negative integers and $\omega_c = eH/cm_{\perp}$ is the cyclotron frequency. The energy levels $\epsilon_{n_1 n_2}$ given by Eqs. (16) and (17) transform to the Fock-Darwin levels³⁹ in the symmetric case $\omega_1 = \omega_2 = \omega_0$ (i.e., isotropic Fermi surface) with

$$\omega_{\pm}^s = \frac{1}{2} (\omega_c^2 + 4\omega_0^2)^{1/2} \pm \omega_c. \quad (18)$$

In the following we discuss the results of our calculations for bismuth nanowires with different orientations of the crystallographic axes with respect to the axis of the wire. In our calculations we use the following values for the diagonal elements of the mass tensor:⁴⁰ m_0 , $0.02m_0$, and $0.006m_0$. We use 0.012 eV for the Fermi energy and $g^* = 50$ for the g factor [the effective g factor for bismuth is of the order of m_0/m_{\perp} (Ref. 37)].

In Fig. 5 we show (a) the conductance and (b) the cohesion force as a function of the length of a bismuth nanowire for different values of an applied magnetic field. The conductance of the wire decreases with the length as the radius of the narrowest part of the wires decreases, thus reducing the number of the conducting electronic channels in the bottleneck of the constriction. The cohesive force oscillates as a function of the length of the wire in correspondence with the changes in the conductance. Note that for stronger applied magnetic fields the values for the conductance, as well as the amplitude of the cohesive force, are smaller since a smaller number of conducting channels exists (below E_F) in the narrowest part of the constriction. The main effect of the magnetic field on the force is to modify the oscillatory pattern [which exists already in zero field; see the solid line in Figs. 5(a) and 5(b)], including the appearance of new peaks. This effect, which is correlated with variations in the wire's conductance [compare panels (a) and (b)], originates from

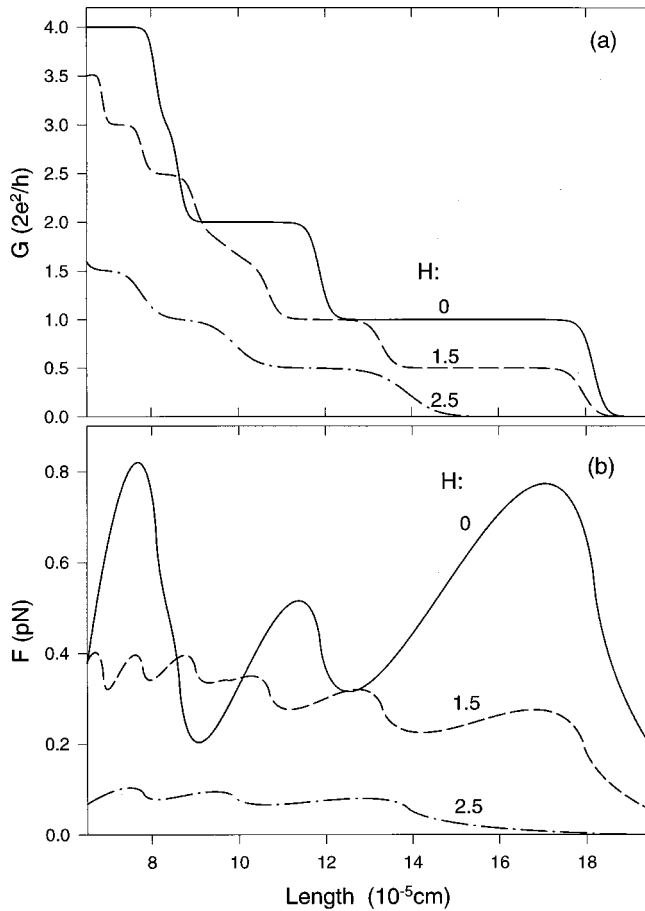


FIG. 5. (a) Conductance (G , in units of $2e^2/h$) and (b) cohesive force (F , in pN) of a bismuth wire, modeled via a soft-wall confining potential with a variable shape, plotted vs the length of the wire, L (in units of 10^{-5} cm). The different curves correspond to the marked values of the applied longitudinal (i.e., directed along the axis of the wire) magnetic field (in units of tesla, T). The Fermi energy for bismuth was taken to be 0.012 eV. The diagonal element of the mass tensor corresponding to the direction along the axis of the wire is $m_{\parallel}=m_0$, and the effective g factor used in our calculations is 50. As the wire elongated its profile was readjusted [see Eq. (6)] such that its volume ($V=2.13\times 10^{-14}$ cm 3) and the radius of its maximal cross section ($R_{\max}=1.02\times 10^{-5}$ cm) remained constant. The geometry of the wire is shown in Fig. 1(b).

magnetic-field-induced removal of both orbital and spin degeneracies and shifts of the electronic transverse energy levels in the nanowire.

In Fig. 6 we show as a function of the strength of the applied magnetic field, (a) the conductance and (b) the cohesion force for wires of different lengths, oriented such that their largest (m_0) diagonal element of the mass tensor corresponds to the axis of the wire. All wires in Fig. 6 have the same volume and the radius, R_{\max} , at the end of the constriction. The behavior of the conductance as a function of the magnetic field demonstrates a “magnetic switch” effect discussed by us previously.²⁹ The pattern of variation of the cohesion force correlates with the step pattern of the conductance. From comparison of the different curves in Fig. 6 we observe that wires with a larger number of conductance channels exhibit a higher sensitivity to the magnetic field. Note the appearance of conductance steps with a magnitude

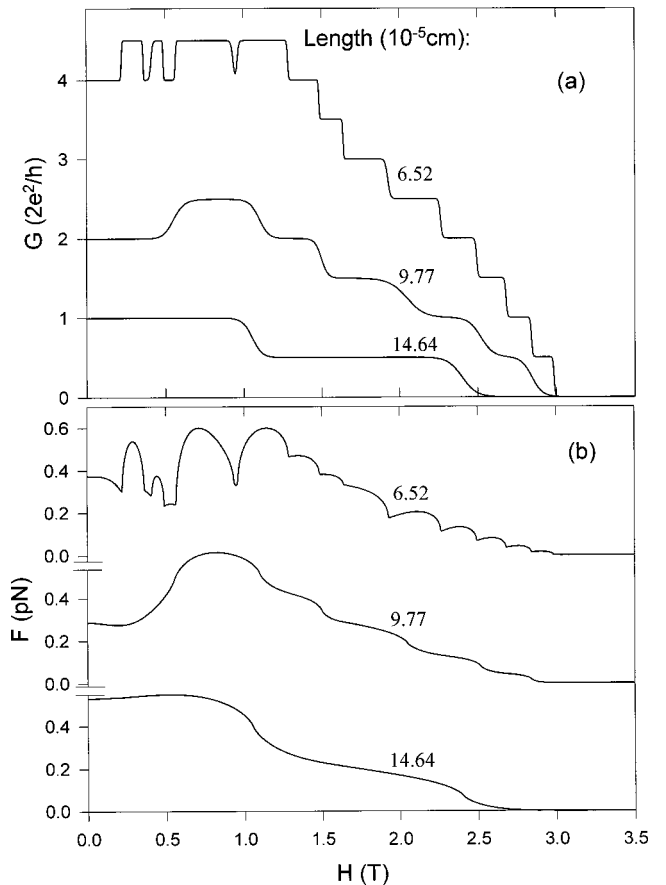


FIG. 6. (a) Conductance (G , in units of $2e^2/h$) and (b) cohesive force (F in pN) of the bismuth wire described in Fig. 5 plotted vs the magnitude of the applied longitudinal magnetic field (in units of tesla, T). The different curves correspond to the marked values of the length of the wire (in units of 10^{-5} cm).

of e^2/h rather than $2e^2/h$ due to removal of the degeneracy of the electron energy levels by the Zeeman spin splitting.

The calculations of the cohesion force and of the conductance presented above pertain to bismuth wires oriented such that the largest diagonal element of the electron-mass tensor coincides with the axis of the wire ($m_{\parallel}=m_0$). In this case the amplitude of the cohesion force is maximal. Indeed, it may be shown easily that the cohesion force behaves as

$$F \sim m_{\parallel}^{1/2} / (m_{\perp}^{3/2} R_0^3). \quad (19)$$

Since for a wire with a fixed number of conducting channels, $R_0 \sim 1/m_{\perp}^{3/2}$, one obtains $F \sim \sqrt{m_{\parallel}}$. This estimate demonstrates enhancement (order of magnitude) of the amplitude of the cohesion force oscillations in the wires where m_{\parallel} is maximal (m_0) compared to the wires where m_{\parallel} is minimal ($0.006m_0$). For bismuth nanowires with a fixed transverse dimension the influence of the crystallographic axis orientation will have an even more profound effect on the electronic transport and cohesion force. Indeed, for a fixed value of R_0 we find that the amplitude of the force oscillations will be 3 orders of magnitude larger for wires with their crystallographic axis corresponding to the largest diagonal element of the mass tensor oriented along the axis of the wire, compared to wires where such a crystallographic axis is perpendicular to the axis of the wire. The crystallographic axis orientation

will also affect the electronic transport through the nanowire since m_{\perp} , as well as the strong anisotropy, will define the number of conducting channels in the narrowest part of the nanowire. We also note that wires with smaller m_{\perp} are more sensitive to the magnetic field and are much better candidates for the demonstration of the influence of an applied magnetic field on the electronic quantum transport; wires with such a crystallographic axis orientation may exhibit “magnetic blockade” of the quantum electronic transport²⁹ at rather modest magnetic field values.

V. SUMMARY

The model analysis that we performed demonstrates that the elongation process in nanowires may be influenced by external parameters such as a magnetic field and/or an applied bias voltage. We studied magnetomechanical properties in nanowires modeled via hard- and soft-wall confining potentials. In both cases oscillations of the cohesive force occur when the quantized conductance of the wire changes from one conductance plateau to another. The soft-wall potential model allows an analytical analysis of the magnetocohesion and is applicable to metals with a strong anisotropy of the Fermi surface. We have shown that the amplitude of the cohesive force oscillations depends on the orientation of the crystallographic axes with respect to the axis of the nanowire. For special orientations of the crystallographic axis the force oscillations might be substantially enhanced. For bis-

muth nanowires with approximately the same number of conducting channels the amplitude of the cohesion force is about an order of magnitude larger if the largest diagonal element of the mass tensor lies along the axis of the wire as compared to wires where that crystallographic axis is perpendicular to the symmetry axis of the wire. Additionally, the soft-wall potential model for nanowire may be generalized for calculations with arbitrary orientation of the magnetic field; for a similar analysis of the magnetoconductance with an arbitrary orientation of the applied magnetic field see Refs. 28, 30, and 41.

Experimental investigations of cohesive force fluctuations are of importance because they allow probing of aspects pertaining to electronic contributions to the cohesive force arising during an elongation process of the nanowires. Such effects may be observed more easily in semimetallic nanowires with the use of magnetic fields with fluxes of the order of the flux quantum; e.g., for a bismuth nanowire with a few transverse electronic modes (that is, Bi wires with radii of ~ 20 –50 nm) this corresponds to readily available magnetic fields of several teslas.

ACKNOWLEDGMENTS

This study is supported by the U.S. Department of Energy, Grant No. FG05-86ER45234. Calculations were performed at the Georgia Tech Center for Computational Materials Science.

-
- ¹U. Landman, W. D. Luedtke, N. A. Burnhan, and R. J. Colton, *Science* **248**, 454 (1990).
- ²See reviews in *Nanowires*, edited by P. A. Serena and N. Garcia (Kluwer, Dordrecht, 1997).
- ³(a) J. I. Pascual, J. Mendez, J. Gomez-Herrero, A. M. Baro, N. Garcia, and Vu Thien Binh, *Phys. Rev. Lett.* **71**, 1852 (1993); (b) J. I. Pascual, J. Mendez, J. Gomez-Herrero, A. M. Baro, N. Garcia, U. Landman, W. D. Luedtke, E. N. Bogacheck, and H.-P. Cheng, *Science* **267**, 1793 (1995); (c) *J. Vac. Sci. Technol. B* **13**, 1280 (1995).
- ⁴N. Agrait, J. G. Rodrigo, and S. Vieira, *Phys. Rev. B* **47**, 12 345 (1993); N. Agrait, G. Rubio, and S. Vieira, *Phys. Rev. Lett.* **74**, 3995 (1995); G. Rubio, N. Agrait, and S. Vieira, *ibid.* **76**, 2302 (1996).
- ⁵L. Olesen, E. Laegsgaard, I. Stensgaard, F. Besenbacher, J. Schiottz, P. Stoltze, K. W. Jacobsen, and J. K. Norskov, *Phys. Rev. Lett.* **72**, 2251 (1994); K. Hansen, E. Laegsgaard, I. Stensgaard, and F. Besenbacher, *Phys. Rev. B* **56**, 2208 (1997).
- ⁶C. J. Muller, J. M. van Ruitenbeek, and L. J. de Jongh, *Phys. Rev. Lett.* **69**, 140 (1992); J. M. Krans, J. M. van Ruitenbeek, V. V. Fisun, I. K. Yanson, and L. J. de Jongh, *Nature (London)* **375**, 767 (1995); A. I. Yanson, G. Rubio Bollinger, H. E. van der Brom, N. Agrait, and J. M. van Ruitenbeek, *Nature (London)* **395**, 783 (1998).
- ⁷D. P. E. Smith, *Science* **269**, 371 (1995).
- ⁸J. L. Costa-Kramer, N. Garcia, P. Garcia-Mochales, and P. A. Serena, *Surf. Sci.* **342**, L1144 (1995).
- ⁹U. Landman, W. D. Luedtke, B. E. Salisbury, and R. L. Whetten, *Phys. Rev. Lett.* **77**, 1362 (1996).
- ¹⁰A. Stalder and U. Durig, *Appl. Phys. Lett.* **68**, 637 (1996).
- ¹¹W. A. DeHeer, S. Frank, and D. Ugarte, *Z. Phys. B: Condens. Matter* **104**, 469 (1997).
- ¹²C. Z. Li and N. J. Tao, *Appl. Phys. Lett.* **72**, 894 (1998); C. Z. Li, H. Sha, and N. J. Tao, *Phys. Rev. B* **58**, 6775 (1998).
- ¹³H. Ohnishi, Y. Kondo, and K. Takayanagi, *Nature (London)* **395**, 780 (1998).
- ¹⁴E. N. Bogacheck, A. M. Zagorskin, and I. O. Kulik, *Fiz. Nizk. Temp.* **16**, 1404 (1990) [Sov. J. Low Temp. Phys. **16**, 796 (1990)].
- ¹⁵T. N. Todorov and A. P. Sutton, *Phys. Rev. Lett.* **70**, 2138 (1993).
- ¹⁶M. Brandbyge, K. W. Jacobsen, and J. K. Norskov, *Phys. Rev. B* **55**, 2637 (1997).
- ¹⁷R. N. Barnett and U. Landman, *Nature (London)* **387**, 788 (1997).
- ¹⁸H. Hakkinen, R. N. Barnett, and U. Landman, *J. Phys. Chem. B* **103**, 8814 (1999).
- ¹⁹C. Yannouleas and U. Landman, *J. Phys. Chem. B* **101**, 5780 (1997).
- ²⁰C. Yannouleas, E. N. Bogacheck, and U. Landman, *Phys. Rev. B* **57**, 4872 (1998).
- ²¹N. Zabala, M. J. Puska, and R. M. Nieminen, *Phys. Rev. B* **59**, 12 652 (1999).
- ²²C. A. Stafford, D. Baeriswyl, and J. Burki, *Phys. Rev. Lett.* **79**, 2863 (1997).
- ²³J. M. van Ruitenbeek, M. H. Devoret, D. Esteve, and C. Urbina, *Phys. Rev. B* **56**, 12 566 (1997).
- ²⁴S. Blom, H. Olin, J. L. Costa-Kramer, N. Garcia, M. Jonson, P. A. Serena, and R. I. Shekhter, *Phys. Rev. B* **57**, 8830 (1998).
- ²⁵A. M. Zagorskin, *Phys. Rev. B* **58**, 15 827 (1998).

- ²⁶C. Hoppler and W. Zwerger, Phys. Rev. B **59**, R7849 (1999).
- ²⁷E. N. Bogacheck, M. Jonson, R. I. Shekhter, and T. Swahn, Phys. Rev. B **47**, 16 635 (1993); **50**, 18 341 (1994).
- ²⁸A. G. Scherbakov, E. N. Bogacheck, and U. Landman, Phys. Rev. B **53**, 4054 (1996).
- ²⁹E. N. Bogacheck, A. G. Scherbakov, and U. Landman, Phys. Rev. B **53**, R13 246 (1996).
- ³⁰A. G. Scherbakov, E. N. Bogacheck, and U. Landman, Phys. Rev. B **57**, 6654 (1998).
- ³¹J. I. Pascual, J. A. Torres, and J. J. Saenz, Phys. Rev. B **55**, R16 029 (1997).
- ³²E. N. Bogacheck, A. G. Scherbakov, and U. Landman, Phys. Rev. B **56**, 14 917 (1997).
- ³³S. Blom, L. Y. Gorelik, M. Jonson, R. I. Shekhter, A. G. Scherbakov, E. N. Bogacheck, and U. Landman, Phys. Rev. B **58**, 16 305 (1998).
- ³⁴E. N. Bogacheck, A. G. Scherbakov, and U. Landman, Phys. Rev. B **54**, R11 094 (1996).
- ³⁵E. N. Bogacheck, A. G. Scherbakov, and U. Landman, Solid State Commun. **108**, 851 (1998); Phys. Rev. B **60**, 11 678 (1999).
- ³⁶The conductance in a magnetic field is calculated using the formalism developed in Refs. 29 and 30.
- ³⁷D. Shoenberg, *Magnetic Oscillations in Metals* (Cambridge University Press, Cambridge, 1984), Chap. 9.
- ³⁸B. Schuh, J. Phys. A **18**, 803 (1985).
- ³⁹V. Fock, Z. Phys. **47**, 446 (1928); C. G. Darwin, Proc. Cambridge Philos. Soc. **27**, 86 (1930).
- ⁴⁰J. E. Aubrey and R. G. Chambers, J. Phys. Chem. Solids **3**, 128 (1957).
- ⁴¹N. G. Galkin, V. A. Geyler, and V. A. Margulis, Zh. Eksp. Teor. Fiz. **117**, 593 (2000) [JETP **90**, 517 (2000)].